Publication Year	2020
Acceptance in OA	2025-02-25T10:05:35Z
Title	Progress on the UV-VIS arm of SOXS
Authors	Rubin, Adam, Ben-Ami, Sagi, Hershko, Ofir, Rappaport, Michael, Gal-Yam, Avishay, Bruch, Rachel, CAMPANA, Sergio, CLAUDI, Riccardo, SCHIPANI, Pietro, ALIVERTI, Matteo, BARUFFOLO, Andrea, BIONDI, FEDERICO, CAPASSO, Giulio, COSENTINO, Rosario, D'ALESSIO, Francesco, D'AVANZO, Paolo, Kuncarayakti, Hanindyo, LANDONI, Marco, MUNARI, MATTEO, Pignata, Giuliano, SCUDERI, Salvatore, VITALI, Fabrizio, Young, David, Achrén, Jani, ARAIZA DURAN, Jose Antonio, Arcavi, Iair, BRUCALASSI, Anna, CAPPELLARO, Enrico, COLAPIETRO, Mirko, DELLA VALLE, Massimo, DE PASCALE, Marco, DI BENEDETTO, Rosario, D'ORSI, SERGIO, Flügel-Paul, Thomas, GENONI, Matteo, Hernandez, Marcos, Kotilainen, Jari, LI CAUSI, Gianluca, Mattila, Seppo, RADHAKRISHNAN SANTHAKUMARI, KALYAN KUMAR, RICCI, Davide, RIVA, Marco, Sadlowski, Susann, SALASNICH, Bernardo, Smartt, Stephen, Sanchez, Ricardo Zanmar, Stritzinger, Maximilian, PEREZ VENTURA, HECTOR
Publisher's version (DOI)	10.1117/12.2560644
Handle	http://hdl.handle.net/20.500.12386/36185
Serie	PROCEEDINGS OF SPIE
Volume	11447

Progress on the UV-VIS arm of SOXS

Adam Rubin[a*], Sagi Ben-Ami[b], Ofir Hershko[b], Michael Rappaport[b], Avishay Gal-Yam[b], Rachel Bruch[b], Sergio Campana[c], Riccardo Claudi[d], Pietro Schipani[e], Matteo Aliverti[c], Andrea Baruffolo[d], Federico Biondi[f], Giulio Capasso[e], Rosario Cosentino[g,h], Francesco D'Alessio[i], Paolo D'Avanzo[c], Hanindyo Kuncarayakti[j,k], Marco Landoni[c], Matteo Munari[h], Giuliano Pignata[l,m], Salvatore Scuderi[n,h], Fabrizio Vitali[i], David Young[o], Jani Achrén[p], José Antonio Araiza-Duran[q,m], Iair Arcavi[r], Anna Brucalassi[l,s], Enrico Cappellaro[d], Mirko Colapietro[e], Massimo Della Valle[e], Marco De Pascale[d], Rosario Di Benedetto[h], Sergio D'Orsi[e], Thomas Flügel-Paul[t], Matteo Genoni[c], Marcos Hernandez[g], Jari Kotilainen[k,j], Gianluca Li Causi[u], Seppo Mattila[j], Kalyan Radhakrishnan[d], Davide Ricci[d], Marco Riva[c], Susann Sadlowski[t], Bernardo Salasnich[d], Stephen Smartt[o], Ricardo Zanmar Sanchez[h], Maximilian Stritzinger[v], and Hector Ventura[g]

[a]European Southern Observatory, Garching bei München, Germany
[b]Weizmann Institute of Science, Rehovot, Israel
[c]INAF - Osservatorio Astronomico di Brera, Merate, Italy
[d]INAF - Osservatorio Astronomico di Padova, Padua, Italy
[e]INAF - Osservatorio Astronomico di Capodimonte, Naples, Italy
[f]Max-Planck-Institut für Extraterrestrische Physik, Garching, Germany
[g]INAF - Fundación Galileo Galilei, Breña Baja, Spain
[h]INAF - Osservatorio Astrofisico di Catania, Catania, Italy
[i]INAF - Osservatorio Astronomico di Roma, Rome, Italy
[j]Tuorla Observatory, Department of Physics and Astronomy, University of Turku, Turku, Finland
[k]FINCA - Finnish Centre for Astronomy with ESO, Turku, Finland
[l]Universidad Andres Bello, Santiago, Chile
[m]Millennium Institute of Astrophysics (MAS), Santiago, Chile
[n]INAF - Istituto di Astrofisica Spaziale e Fisica Cosmica, Milano, Italy
[o]Queen's University Belfast, Belfast, UK
[p]Incident Angle Oy, Turku, Finland
[q]Centro de Investigaciones en Optica A. C., León, Mexico
[r]Tel Aviv University, Tel Aviv, Israel
[s]INAF-Osservatorio Astrofisico Arcetri, Firenze, Italy
[t]Fraunhofer-Institut für Angewandte Optik und Feinmechanik IOF, Jena, Germany
[u]INAF - Istituto di Astrofisica e Planetologia Spaziali, Rome, Italy
[v]Aarhus University, Aarhus, Denmark

ABSTRACT

We present our progress on the UV-VIS arm of Son Of X-Shooter (SOXS), a new spectrograph for the NTT. Our design splits the spectral band into four sub-bands that are imaged onto a single detector. Each band uses an optimized high efficiency grating that operates in 1st order (m=1). In our previous paper we presented the concept and preliminary design. SOXS passed a Final Design Review in July 2018 and is well into the construction

*arubin@eso.org

Ground-based and Airborne Instrumentation for Astronomy VIII, edited by Christopher J. Evans, Julia J. Bryant, Kentaro Motohara, Proc. of SPIE Vol. 11447, 114475L · © 2020 SPIE · CCC code: 0277-786X/20/$21 · doi: 10.1117/12.2560644

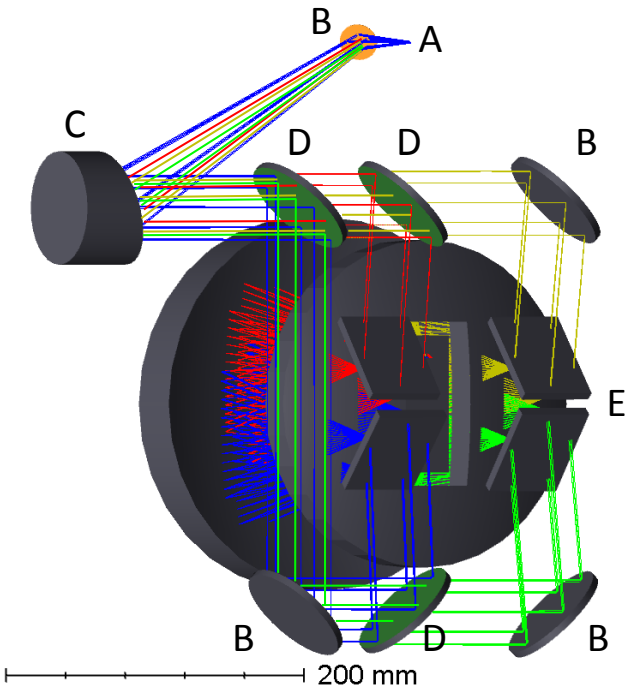

Figure 1. System layout: A. slit plane, B. Reflective mirrors, C. OAP Collimator, D. Dichroic filters, E. Gratings.

phase. Here we present the final design, performances of key manufactured elements, and the progress in the assembly. Based on the as-built elements, the expected throughput of the visual arm will be $> 55\%$. This paper is accompanied by a series of contributions describing the progress made on the SOXS instrument.

Keywords: spectrograph, transients

1. INTRODUCTION

The Son Of X-Shooter (SOXS)[1–3] is a medium resolution spectrograph ($R \sim 4500$ for a 1 arcsecond slit) proposed for the ESO 3.6 m NTT. SOXS is comprised of a common path, which splits the incoming light to a UV-VIS arm ($0.35 - 0.85$ μm) and a NIR arm ($0.8 - 2.0$ μm), an acquisition camera, and a calibration unit—all of which are described in other papers in these proceedings.[3–15]

The visual arm has a novel design, which was described in our previous paper.[16] The beam is divided into four bands and imaged by a single camera. Each band makes use of a high efficiency grating in first order ($m = 1$) to increase the photon efficiency. The optical layout is shown in Figure 1. The UV-VIS spectrograph has two separated levels, one called the "feed", where the source image is collimated, split with dichroics and mirrors, and dispersed by the gratings. The feed layout is shown in Figure 2. The dispersed beam is directed to the lower stage which is comprised of a single camera which images all beams onto one detector. The camera is made up of a CaF2 corrector, a fused silica mirror and a fused silica field flattener—each having one aspheric surface. The camera layout is shown in Figure 3.

In the period between the previous paper and this manuscript the optics—gratings, mirrors, filters, collimator and camera—have been manufactured. Most of the mechanical structure has been manufactured, and the continuous flow cryostat and vacuum vessel are currently being tested. The system is now in the assembly, integration and verification phase with work ongoing. The entire SOXS system is currently scheduled to undergo preliminary acceptance in Europe by the end of 2021.

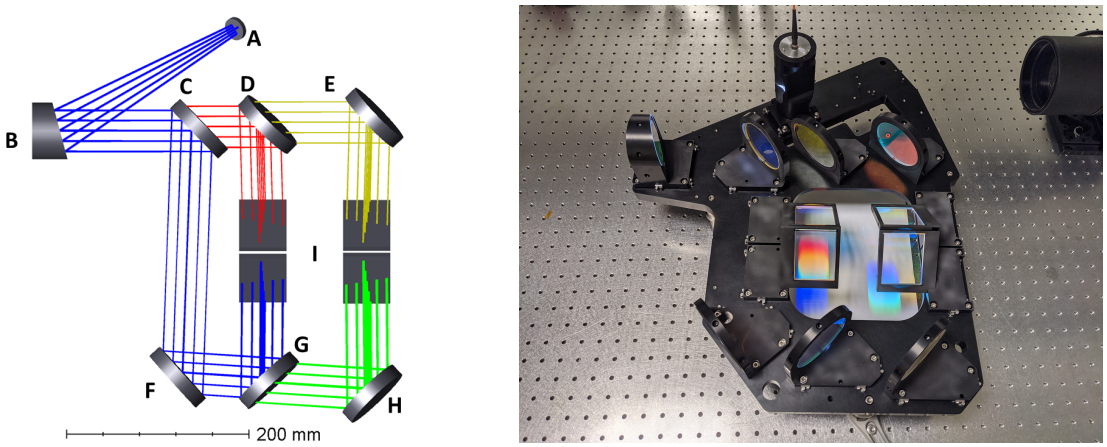

Figure 2. Left: Layout of the feed. A: Folding mirror; B: Off-axis parabola collimator; C/D/G: Dichroic mirrors dividing $u+g$ from $r+i$, r from i, and u from g, respectively; E/F/H: Dielectric mirrors reflecting i, $u+g$, and g, respectively; I: gratings. Right: the as-built feed illuminated withe a white light source.

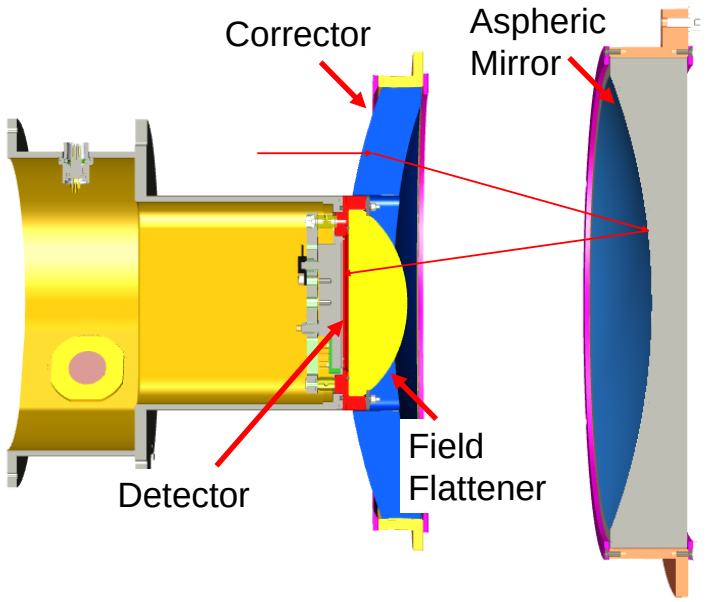

Figure 3. Camera layout. An illustration of the light path is shown in red.

Table 1. SOXS UV-VIS and grating parameters.

Quasi-Order	Wavelength Range [nm]	Line Density [lines/mm]	AOI	$\lambda_{Littrow}$ [nm]
u	$350 - 440$	3378.4	41°	388.4
g	$427 - 547$	2652.5	41°	494.7
r	$527.5 - 680$	2118.6	41°	619.3
i	$664 - 850$	1709.4	41°	767.6

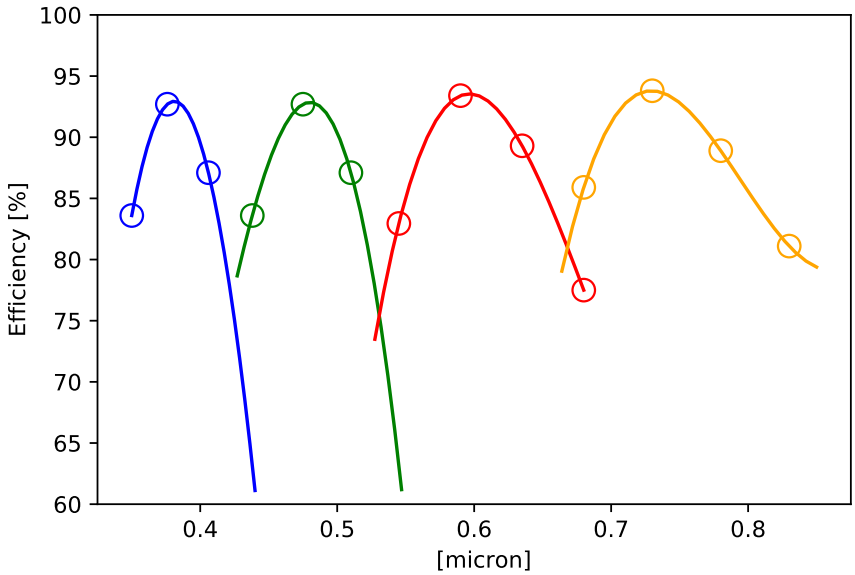

Figure 4. SOXS visual arm as-built grating efficiencies as measured by the manufacturer. The average between the polarizations is shown. The lines are a third-order polynomial fit to the data.

2. AS-BUILT PERFORMANCE OF ELEMENTS

2.1 Gratings

The four gratings for the SOXS visual arm, produced by using atomic layer deposition on fused silica, were manufactured by Fraunhofer IOF, Jena. Their parameters are given in Table 1. Figure 4 shows the average efficiency (between TM and TE polarizations) for the four gratings. Figure 5 shows the u-band grating in its mount and gluing jig. The general procedure for mounting the small optics into their mounts is describe in section 4.

2.2 Off-axis parabola

The off-axis parabola collimator was manufactured by Winlight System. The parabola has a 30 degree off-axis angle and a design radius of 545.11 mm. The parabola was manufactured with within ±0.015% of the design radius and with an RMS surface figure error of $\sim$ 20 nm.

2.3 Mirrors and dichroic filters

The flat mirrors and dichroic filters used in the feed were manufactured by Asahi Spectra to $\lambda/8$ flatness. The mirrors and filters were measured by the manufacturer at their design angle of incidence. The average reflectance for all was $>$ 99% and transmission for the filters was measured to be $>$ 98%. One of the most challenging elements was element A (fold mirror toward the collimator, see Figure 2). This element reflects the entire spectrum, and receives an incident F/6.5 beam at 45°. As a result, the requirements were for good spectral reflectivity over the entire spectrum for angles of incidence ranging from 41 to 49 degrees. The element

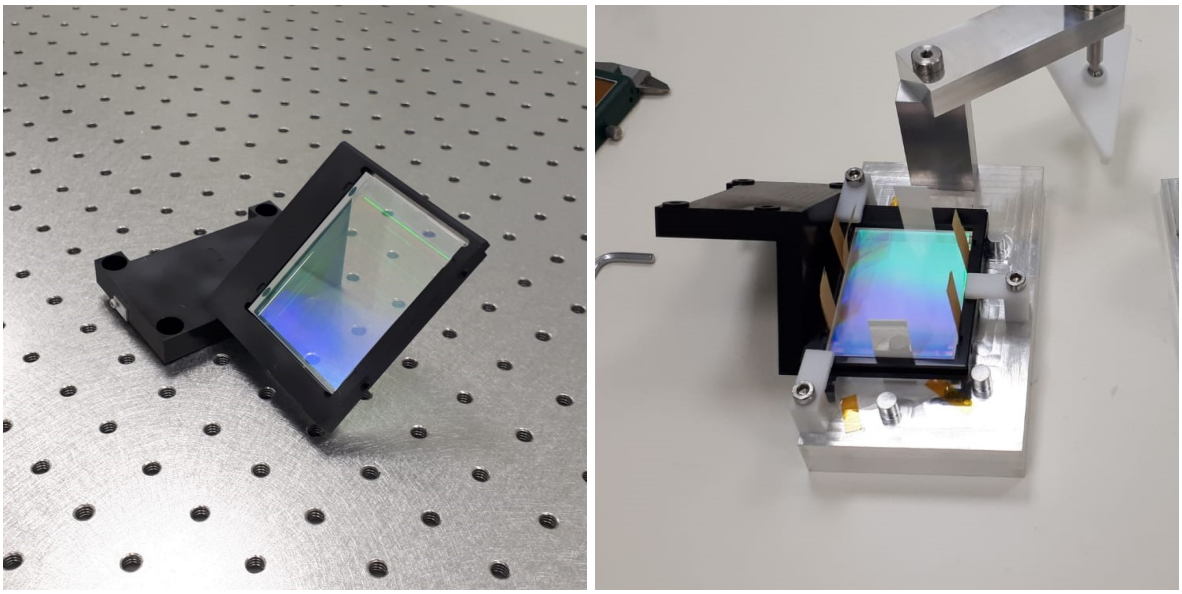

Figure 5. Grating adhered in its mount (left) and in the gluing jig (right). Shims were used to center the element during the gluing process and to ensure the correct thickness of RTV at each adhesion point.

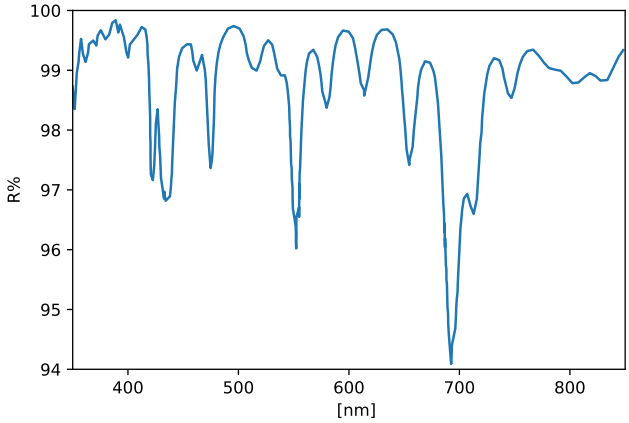

Figure 6. Measured reflection efficiency of the off-axis parabola.

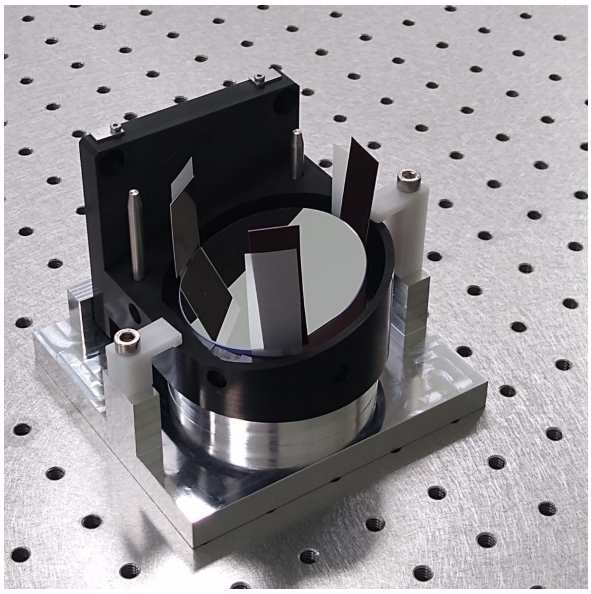

Figure 7. Off-axis parabola in its gluing jig.

was measured under these conditions and satisfied average reflectance above 99% over the relevant spectral range and angles of incidence. For the full response of each of the elements, see Figures 8 and 9.

Element	Diameter [mm]	Reflected [nm]	Transmitted [nm]	Transition [nm]
A	25.4	$350 - 850$	-	-
C	76.2	$350 - 527.5$	$547 - 850$	$527.5 - 547$
D	76.2	$527.5 - 664$	$680 - 850$	$664 - 680$
E	76.2	$664 - 850$	-	-
F	76.2	$350 - 547$	-	-
G	76.2	$350 - 427$	$440 - 547$	$427 - 440$
H	76.2	$427 - 547$	-	-

Table 2. Specifications for the filters and mirrors manufactured by Asahi. Element labels match the ones that appear in Figure 2.

2.4 Camera

The camera optics are manufactured by Winlight System. The camera is comprised of a CaF2 corrector, a fused silica mirror, and a fused silica field flattener—each with one aspheric surface. The field flattener serves as the detector window. The camera layout is shown in Figure 3. The elements were manufactured to tolerance, with excellent RMS figure error of < 30 nm, and roughness < 1 nm. As of the writing of this manuscript, the corrector is being re-coated due to a manufacturing process error. However, witness sample measurements have already been performed and a good estimate of the total throughput of the camera can be estimated. The camera has an average photon efficiency of $> 96\%$ and is shown in Figure 10.

3. MECHANICAL STRUCTURE

The mechanical structure and mounts for the feed and small optics (filters, mirrors and gratings) have been manufactured. The Invar truss which holds the camera optics is in advanced stages of production.

With the final design in hand, a flexure analysis showed that we expect less than one pixel motion due to flexure of the UV-VIS spectrograph. SOXS will be mounted on the Nasmyth flange of the NTT. Therefore it is expected to rotate during observations, inducing a strongly varying gravity load. We performed a flexure analysis to estimate the displacement of the spectrum at different instrument orientations. We performed a finite

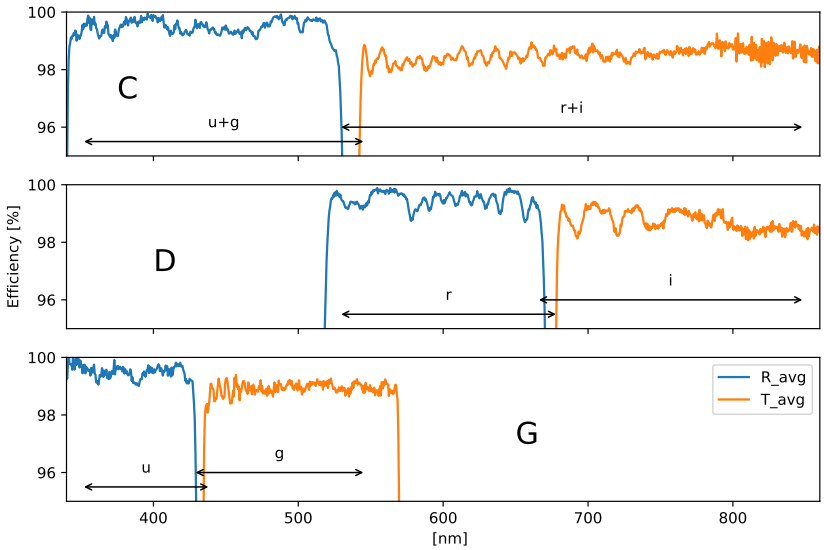

Figure 8. From the top: transmission and reflection of the dichroic filter which splits the light between the $u+g$ and $r+i$ bands, between the u and g bands, and between the r and i bands, as measured by the manufacturer. Arrows mark the region that falls on the detector in each band. The plots are labeled according to the labels in Figure 2.

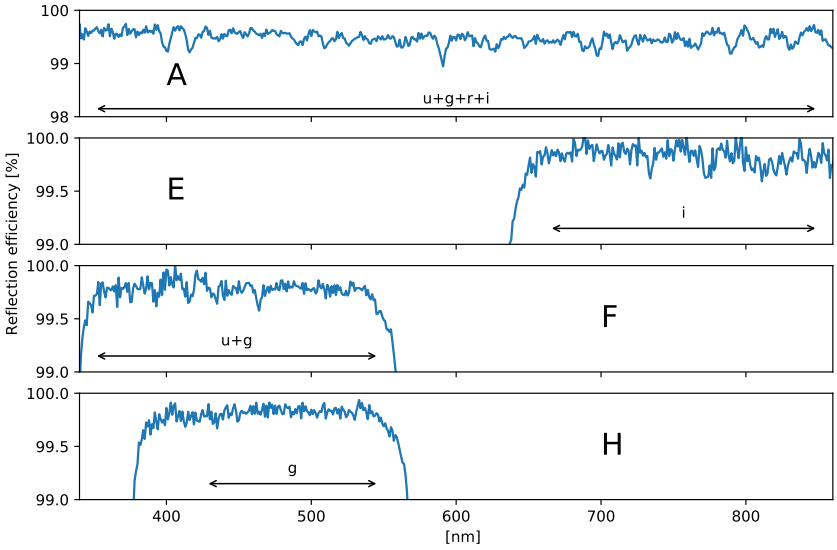

Figure 9. Measured reflection efficiencies for the feed mirrors manufactured by Asahi. Arrows mark the region that falls on the detector in each band. The plots are labeled according to the labels in Figure 2.

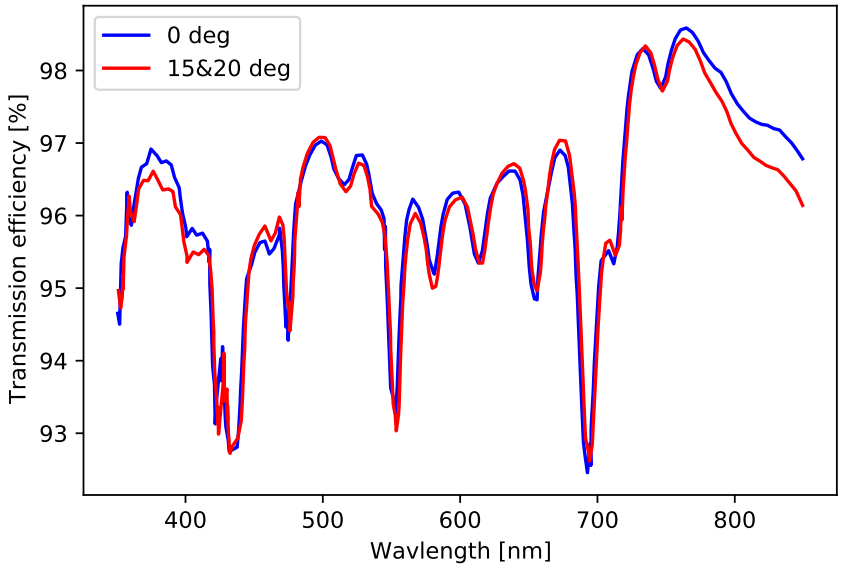

Figure 10. Measured transmission for the entire camera: corrector, mirror, and field flattener. The average efficiency is $> 96\%$.

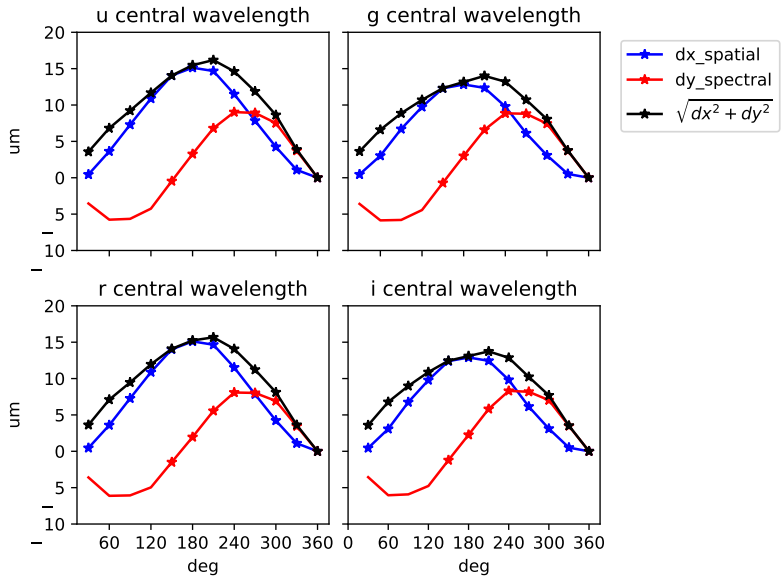

Figure 11. Shift of the spectrum on the detector due to rotation of the instrument on the Nasmyth flange.

element analysis in COMSOL Multiphysics®. Each optical element's tilt and displacement were recorded and implemented in Optics Studio. Then the position of the central wavelength was recorded for each orientation of the instrument. The results are shown in Figure 11. Figure 11 shows that for an entire 360 degree rotation the spectrum moves by a total of one pixel. However this scenario requires a long exposure while pointing very close to the zenith and is should occur very rarely.

The vacuum chamber and detector mount were manufactured at the Weizmann Institute. The chamber is internally gold plated to reduce the thermal load on the detector which is cooled with a custom thermal link. The CCD baseplate assembly is shown in Figure 12. The CCD is model e2V CCD44-82 and will be operated

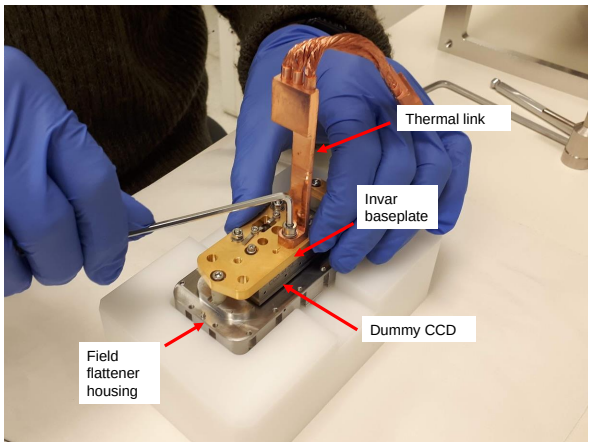

Figure 12. Field flatenner housing, dummy CCD, Invar baseplate, and copper thermal link.

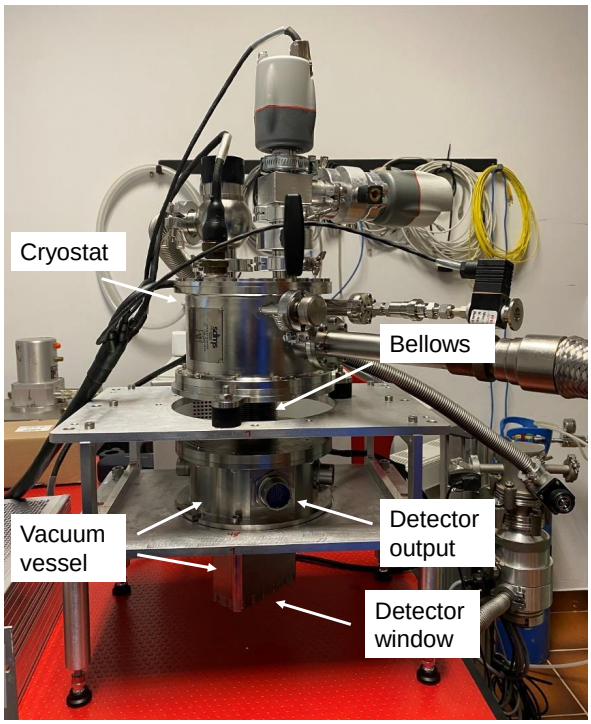

Figure 13. Vacuum chamber and cryostat. A welded bellows separates the cryostat from the vacuum vessel mechanically, preventing flexure due to the weight of the cryostat.

at 170 K. The design of the UV-VIS detector system was described in a previous paper.[17] The progress on the detector system is reported in an accompanying paper in these proceedings.[9] The full assembly is shown in Figure 13 and is currently under test.

4. MOUNTING AND ALIGNMENT

The general alignment and integration strategy is described in a previous paper.[18] The small optics were placed on dedicated jigs which were adjusted using a CMM. Shims were used to center the elements and create gaps of specified width for the RTV adhesion pads. Examples of elements in their jigs are shown in Figures 5 and 7.

The elements which must be aligned to good accuracy are the OAP and the camera elements. The gratings, filters, and mirrors are not sensitive to in-plane displacement, and can be positioned to better than ± 0.1 degrees with the CMM alone.

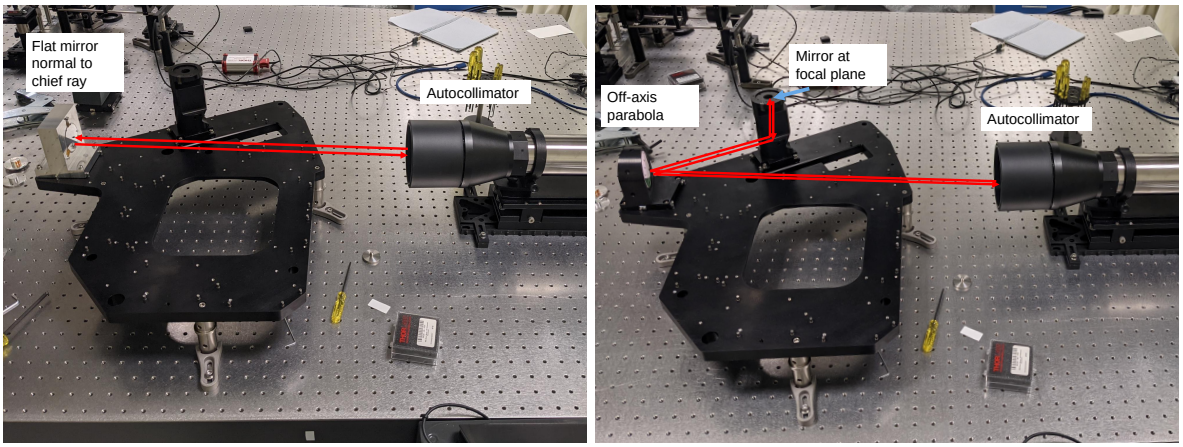

Figure 14. Alignment setup for slit position. Left, stage $1-2$: alignment of the autocollimator to the direction of the design chief ray. Right, stages $3-5$: adjustment of the focal plane mirror height to achieve a return cross that is in focus.

The OAP was placed accurately with a CMM and was considered a datum for the remainder of the feed alignment. The main alignment task was to accurately determine the focal plane of the OAP. The determination of the focal plane followed the following procedure:

1. Place flat mirror, in place of OAP, normal to the design chief ray. Ensure accurate positioning with a CMM and shim accordingly.
2. Align the autocollimator against the flat mirror to sub-arcsecond accuracy.
3. Replace flat mirror with OAP.
4. Place flat mirror at design focal point oriented normal to design chief ray. Due to the small size of the mirror the angular accuracy is low, but this induces only vignetting and is irrelevant for this procedure.
5. Observe reflected cross in the autocollimator and shim the retroreflection mirror until the center of the cross is in focus.

5. EXPECTED SYSTEM PERFORMANCE

The throughput of the UV-VIS arm is extremely high. Taking into account the as-built transmission and reflection measurements, the throughput is 79.7%, 59.4%, and 55.7% for the spectrograph optics, optics + detector, and spectrograph + the common path optics respectively. Figure 15 shows the spectral transmission curves as estimated from the single element throughput measurements. The camera and collimator were manufactured well within tolerance, and the enslitted energy diameter is essentially nominal when taking into account the as-built prescription. The enslitted energy with the as-built prescription is shown in Figure 16.

6. FUTURE ACTIVITIES

The camera optics will be shipped by the end of 2020. The UV-VIS spectrograph will then be assembled and tested with an engineering detector at the Weizmann Institute in Q1 of 2021. Following successful operation at the Weizmann Institute the system will be shipped to Padua where it will be integrated with the scientific CCD and the rest of the spectrograph, with preliminary acceptance Europe currently scheduled for end of 2021.

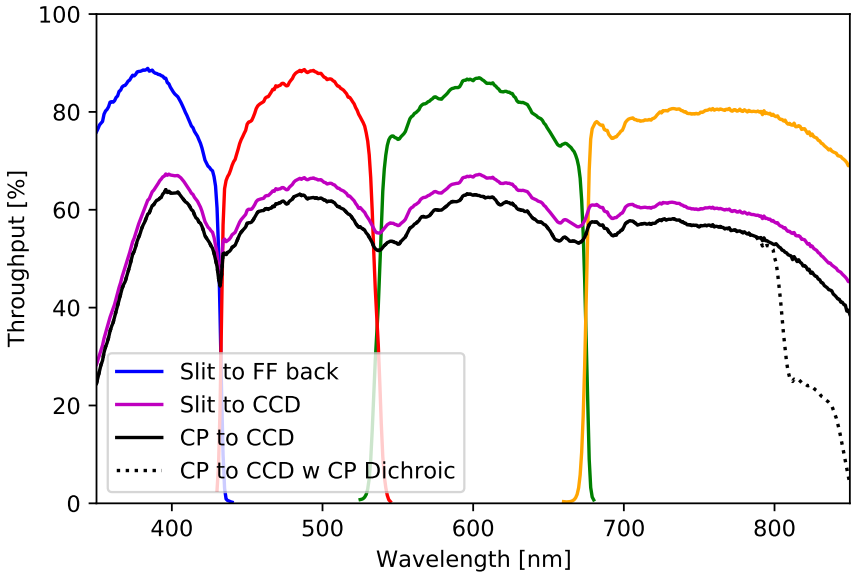

Figure 15. Total estimated efficiency, based on element as-built measurements. The average efficiency of the UV-VIS arm is 79.7%, 59.4%, and 55.7% for the spectrograph optics, optics + detector, and spectrograph + the common path optics respectively.

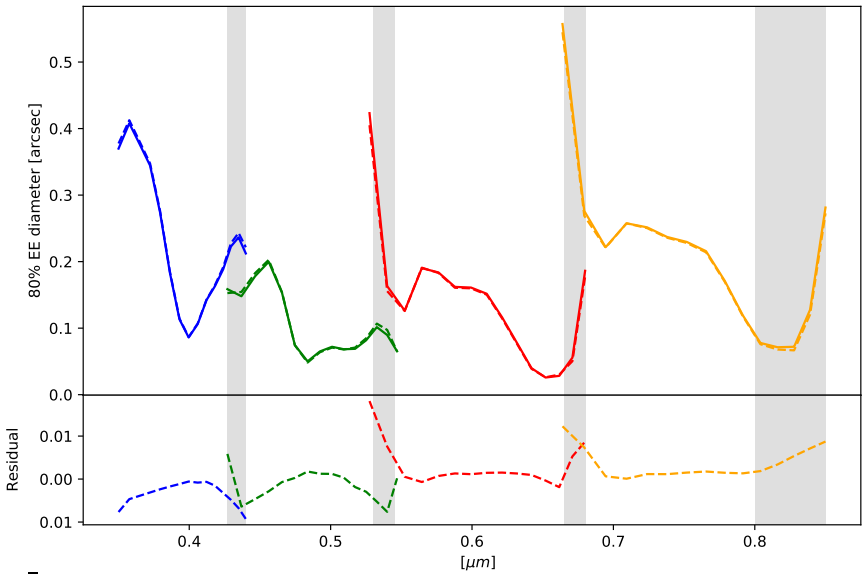

Figure 16. Estimated as-built image quality compared to design. The lower panel shows the difference between the model with the as-built element figures and the nominal design.

λ

REFERENCES

[1] Schipani, P., Claudi, R., Campana, S., et al., "The new SOXS instrument for the ESO NTT," in [*Ground-based and Airborne Instrumentation for Astronomy VI*], **9908**, 990841, SPIE (Aug. 2016).

[2] Schipani, P., Campana, S., Claudi, R., et al., "SOXS: a wide band spectrograph to follow up transients," in [*Ground-based and Airborne Instrumentation for Astronomy VII*], **10702**, 107020F, SPIE (July 2018).

[3] Schipani, P., Campana, S., Claudi, R., et al., "Development status of the SOXS spectrograph for the ESO-NTT telescope," in [*Ground-based and Airborne Instrumentation for Astronomy VIII*], **11447**, 1144709, SPIE (Dec. 2020).

[4] Aliverti, M., Oggioni, L., Genoni, M., et al., "Manufacturing, integration, and mechanical verification of SOXS," in [*Ground-based and Airborne Instrumentation for Astronomy VIII*], **11447**, 114476O, SPIE (Dec. 2020).

[5] Biondi, F., Santhakumari, K. K. R., Claudi, R., et al., "The AIV strategy of the common path of Son Of X-Shooter," in [*Ground-based and Airborne Instrumentation for Astronomy VIII*], **11447**, 114476P, SPIE (Dec. 2020).

[6] Brucalassi, A., Pignata, G., Araiza-Duran, J. A., et al., "Final design and development status of the acquisition and guiding system for SOXS," in [*Ground-based and Airborne Instrumentation for Astronomy VIII*], **11447**, 114475V, SPIE (Dec. 2020).

[7] Claudi, R., Biondi, F., Elias-Rosa, N., et al., "Operational modes and efficiency of SOXS," in [*Ground-based and Airborne Instrumentation for Astronomy VIII*], **11447**, 114477C, SPIE (Dec. 2020).

[8] Colapietro, M., Capasso, G., D'Orsi, S., et al., "Progress and tests on the instrument control electronics for SOXS," in [*Software and Cyberinfrastructure for Astronomy VI*], **11452**, 1145225, SPIE (Dec. 2020).

[9] Cosentino, R., Hernandez, M., Ventura, H., et al., "Development status of the UV-VIS detector system of SOXS for the ESO-NTT telescope," in [*Ground-based and Airborne Instrumentation for Astronomy VIII*], **11447**, 114476C, SPIE (Dec. 2020).

[10] Genoni, M., Landoni, M., Causi, G. L., et al., "SOXS end-to-end simulator: development and applications for pipeline design," in [*Modeling, Systems Engineering, and Project Management for Astronomy IX*], **11450**, 114501B, SPI (Dec. 2020).

[11] Kuncarayakti, H., Achrén, J., Campana, S., et al., "Design and development of the SOXS calibration unit," in [*Ground-based and Airborne Instrumentation for Astronomy VIII*], **11447**, 1144766, SPIE (Dec. 2020).

[12] Ricci, D., Baruffolo, A., Salasnich, B., et al., "Development status of the SOXS instrument control software," in [*Software and Cyberinfrastructure for Astronomy VI*], **11452**, 114522Q, SPIE (Dec. 2020).

[13] Sanchez, R. Z., Aliverti, M., Munari, M., et al., "SOXS: effects on optical performances due to gravity flexures, temperature variations, and subsystems alignment," in [*Ground-based and Airborne Instrumentation for Astronomy VIII*], **11447**, 114475F, SPIE (Dec. 2020).

[14] Vitali, F., Aliverti, M., Capasso, G., et al., "The development status of the NIR Arm of the new SoXS instrument at the ESO/NTT telescope," in [*Ground-based and Airborne Instrumentation for Astronomy VIII*], **11447**, 114475N, SPIE (Dec. 2020).

[15] Young, D. R., Landoni, M., Smartt, S. J., et al., "The SOXS data-reduction pipeline," in [*Software and Cyberinfrastructure for Astronomy VI*], **11452**, 114522D, SPIE (Dec. 2020).

[16] Rubin, A., Ben-Ami, S., Hershko, O., et al., "MITS: the multi-imaging transient spectrograph for SOXS," in [*Ground-based and Airborne Instrumentation for Astronomy VII*], **10702**, 107022Z, SPIE (July 2018).

[17] Cosentino, R., Aliverti, M., Scuderi, S., et al., "The VIS detector system of SOXS," in [*Ground-based and Airborne Instrumentation for Astronomy VII*], **10702**, 107022J, SPIE (July 2018).

[18] Biondi, F., Claudi, R., Marafatto, L., et al., "The assembly integration and test activities for the new SOXS instrument at NTT," in [*Ground-based and Airborne Instrumentation for Astronomy VII*], **10702**, 107023D, SPIE (July 2018).